Attenuation Estimation using Spectral Cross-Correlation

Hyungsuk Kim, *Student Member, IEEE*, and Tomy Varghese, *Senior Member, IEEE*

***Abstract*—Estimation of the local attenuation coefficient in soft tissue is important both for clinical diagnosis and for further analysis of ultrasound B-mode images. However, it is difficult to extract spectral properties in a small region of interest from noisy backscattered ultrasound radio frequency (RF) signals. Diffraction effects due to transducer beam focal properties also have to be corrected for accurate estimation of the attenuation coefficient. In this paper, we propose a new attenuation estimation method using spectral cross-correlation between consecutive power spectra obtained from the backscattered RF signals at different depths. Since the spectral cross-correlation method estimates the spectral shift by comparing the entire power spectra, it is more robust and stable to the spectral noise artifacts in the backscattered RF signals. A diffraction compensation technique using a reference phantom with a known attenuation coefficient value is also presented. Local attenuation coefficient estimates obtained using spectral cross-correlation are within 2.3% of the actual value with small estimation variances, as demonstrated in the simulation results.**

I. Introduction

Attenuation estimation in biological tissue with ultrasound pulse-echo systems has been widely studied, because ultrasound attenuation parameters are closely related to the type and pathological state of tissue [1], [2]. Typical B-mode images of ultrasound, however, display only the magnitude of the backscattered radio frequency (RF) signals under the assumption of a constant speed of sound with time-gain compensation (TGC) utilized to compensate for the attenuation properties of the tissue scanned. Nevertheless, pathological changes in tissue may introduce shadowing or enhancement artifacts below highly attenuating or lower attenuating regions in B-mode images, respectively. Attenuation of the ultrasound signals in the B-mode images has been used for detecting diseases in liver [3] and breast [4]. Therefore, estimation of the ultrasonic attenuation properties from typical B-mode images would not only provide useful diagnostic information, but also enable clear interpretation of the B-mode images for further analysis.

Since attenuation in soft tissues generally demonstrates a linear frequency dependence [5], [6], different attenuation estimation methods utilizing this assumption have been reported in the literature. Most of these methods can be classified as either time-domain or frequency-domain approaches.

In the time domain, measurement of the zero crossing density of the RF echo signal [6] has been used for estimating attenuation. Jang *et al.* [7] proposed a method for measuring entropy differences between two adjacent segments of narrowband echo signals. Video or B-mode signal analysis methods have also been developed by Knipp *et al.* [8] to estimate attenuations directly from B-mode images. Baldwin *et al.* [9] estimated myocardial attenuation from M-mode images.

In the frequency domain, there are two basic methods, i.e., the spectral difference or the spectral shift in the power spectrum at different depths, to estimate the attenuation coefficient. While spectral difference approaches [10] calculate the amplitude decay of the backscattered RF signal, spectral shift approaches [11] estimate the downshift in the center frequency from the normalized power spectrum with propagation depth. Since the amplitude of the backscattered RF echo signals depends on both scattering and attenuation, spectral difference approaches are unable to estimate attenuation coefficients accurately at boundaries where backscatter changes occur [12]. Kuc estimated attenuation using the slope of the difference between the logarithm of the echo signal power spectra obtained from different depths in tissue [5]. The use of a linear regression technique using smoothed log power spectra was developed by Wilson *et al.* [13]. The spectral downshift of the center frequency has also been measured by the centroid downshift method proposed by Fink *et al.* [14] using short-time Fourier analysis techniques. The phase lag in the autocorrelation function of complex echo signals [15] and second-order autoregressive models [11], [16] have also been used to estimate the center frequency shift in the power spectrum. The amplitude decay along the beam propagation using narrowband pulses [17] and the amplitude changes in time-frequency representation [10] have been utilized to estimate attenuation. Yao *et al.* [12] developed a method to reduce system and transducer dependencies using a reference phantom whose attenuation parameters are known *a priori*.

In this paper, we present a new frequency-domain method to estimate attenuation in soft tissue using cross-correlation analysis between two power spectra obtained at different depths. While the centroid downshift method estimates the center frequency downshift of the power spectrum by computing the n-th moment of the power spectrum, the spectral cross-correlation (SCC) method

Manuscript received March 23, 2006; accepted November 3, 2006.

The authors are with the Department of Medical Physics and the Department of Electrical and Computer Engineering, The University of Wisconsin-Madison, Madison, WI 53706 (e-mail: hyungsuk@cae.wisc.edu).

Digital Object Identifier 10.1109/TUFFC.2007.274

computes the spectral downshift of the entire power spectrum. The SCC method was first utilized in the direct estimation of tissue strain in elastography by computing the spectral shift in the power spectra of pre- and post-compression RF signals [18].

In addition to the new attenuation estimation method, we also present an algorithm to compensate for diffraction effects with respect to the transducer beam focus. Since most ultrasound pulse-echo systems utilize focusing around the region of interest, diffraction effects have to be taken into account for stable and independent estimation of the attenuation coefficient [19]. We use backscattered RF signals from a reference phantom, with known attenuation parameters, to compensate for diffraction effects. The gated window sizes required for obtaining accurate and stable power spectra using short-time Fourier analysis techniques are also discussed.

The paper is organized as follows. In Section II, a theoretical derivation of the SCC algorithm is presented. An ultrasound simulation program and methods for estimating the characteristics of the transmit pulse from backscattered RF signals are presented in Section III. Compensation for diffraction effects using a reference phantom and selection of appropriate gated window sizes are also described in this section. In Section IV, simulation results that illustrate the performance of the new method are presented, and experimental results are described in Section V. Finally, Section VI summarizes the contributions of this paper.

II. The Spectral Cross-Correlation Algorithm

Most methods that estimate the attenuation coefficient assume a linear frequency dependence of the attenuation and constant speed of sound in the region of interest in order to simplify the ultrasound attenuation model in pulse-echo systems. Other assumptions include weak scattering in tissue, ignoring contributions due to multiple scattering of the transmit pulse (i.e., the Born approximation). Under these assumptions, the intensity of the backscattered RF signal, $R(f,z)$, received at the ultrasound transducer can be expressed as a product of the transmit pulse, attenuation, and backscatter terms in the frequency domain:

$$R(f,z) = G(f) \cdot A(f,z) \cdot B(f), \tag{1}$$

where z denotes the depth of the region of interest from the transducer, and $G(f)$ represents the transmit pulse, which depends on the transducer design. The transmit pulses are, generally, assumed as Gaussian; Wear showed that this Gaussian approximation of the power spectrum was accurate to within 10% in root mean square error analysis [20]. Assuming a Gaussian-shaped envelope for the transmit pulse, we denote it in the frequency domain as

$$G(f) = \exp\left\{-\frac{(f-f_c)^2}{2\sigma^2}\right\}, \tag{2}$$

where f_c is the center frequency and σ^2 is the variance of the transmit pulse. $A(f,z)$ represents the cumulative attenuation in soft tissue. As assumed earlier, the attenuation of most soft tissue is linearly proportional to the frequency in decibels, and is given by

$$A(f,z) = \exp\{-4\beta f z\}, \tag{3}$$

where β is the attenuation coefficient in units of Nepers/cm/MHz.

The backscattered echo signals denoted by $B(f)$ in (1) are modeled as a stochastic process due to the large number of random scatterers in soft tissue [21], [22]. However, for most attenuation estimation approaches in the frequency domain, backscatter models that incorporate only nonlinear frequency-dependent properties are used. Frequency dependence of backscatter is generally modeled as a power of frequency, and expressed in an exponential form of the Taylor series expansion, which is then utilized to derive a closed-form expression for the spectral shift in the frequency domain [6], [23]:

$$\begin{aligned} B(f) = f^n &= \exp\{n \cdot \log(f)\} \\ &= \exp\left\{n \cdot \log(f_c) + n \cdot \log\left(1 + \frac{f-f_c}{f_c}\right)\right\} \\ &\approx f_c^n \cdot \exp\left\{n \cdot \left(\frac{f-f_c}{f_c} - \frac{(f-f_c)^2}{2f_c^2}\right)\right\} \\ &\propto \exp\left\{-\frac{n \cdot (f^2 - 4f_c f)}{2f_c^2}\right\}. \end{aligned} \tag{4}$$

The expression shown in (4) ignores higher-order terms of the Taylor series expansion. The parameter n can vary from 0 for specular scattering to 4 for Rayleigh scattering. Typical values of n for human tissue are between 1 and 2.

The SCC algorithm relies on the measurement of the spectral shift over the entire power spectra obtained at two different depths. The cross-correlation function between two power spectra at different depths is given by

$$S(f_o) = \int_{-\infty}^{\infty} R(f+f_o,\, z_1) R(f,\, z_2) df, \tag{5}$$

where f_o denotes the spectral shift in the center frequency, and z_1 and z_2 ($z_1 < z_2$) are two different depths relative to the transducer. If we assume that local attenuation values do not change abruptly in a small region, and z_1 and z_2 are close to each other, then the attenuation coefficients at depth z_1 and z_2 could be assumed to be similar. Under this assumption, the expression for the spectral shift between the two power spectra using the cross-correlation algorithm (derived as (A16) in the Appendix) is given by

$$f_{o(\max)} = -\frac{4\sigma^2\beta(z_1 - z_2)}{1 + \frac{n\sigma^2}{f_c^2}}. \tag{6}$$

Since the center frequency is generally greater than the square root of the variance of the transmit pulse, and the parameter n for human tissue is between 1 and 2, the

spectral shift between the power spectra obtained at the two different depths is linearly proportional to the product of the attenuation coefficient and to the difference of the depths at which the spectra were obtained. The spectral shift between the two power spectra at depth z_1 and z_2 provides a direct estimate of the attenuation coefficient. The relationship shown in (6) between attenuation and the spectral shift has also been derived by Girault *et al.* [24] using the frequency corresponding to the maximum power in the power spectrum. Differentiating (6) with respect to z, the slope of the spectral shift along depth is proportional to the attenuation coefficient, β. Under the assumption of linear frequency-dependent attenuation in soft tissue, linear regression over the local spectral shift estimates (usually several blocks along the axial direction) is used to compute the final attenuation coefficient.

III. Method

Estimation of the attenuation coefficient in ultrasound pulse-echo systems is based on ascertaining the frequency-dependent attenuation of different frequency components in soft tissue. Because higher frequency components exhibit increased attenuation than lower frequencies, the power spectrum of echo signals obtained using short-time Fourier analysis demonstrates a downward shift (to the lower frequency) in the center frequency with depth. Previous reports in the literature have shown that the attenuation coefficient in soft tissue is almost linearly proportional to the frequency up to 10 MHz [5]. Due to the linear increase in the attenuation with higher frequencies, the slope of the center frequency downshift versus depth is proportional to the attenuation coefficient. Assuming a Gaussian-shaped transmit pulse whose variance is invariant along depth, the relationship between the slope of downshift of the center frequency versus depth and attenuation coefficient is given by

$$\beta(\mathrm{dB/cm/MHz}) = -\frac{8.686}{4\sigma^2} \cdot \frac{df_c(z)}{dz}, \tag{7}$$

where z is the distance of the region of interest from the transducer and σ^2 is the variance of the transmit pulse. The term $f_c(z)$ denotes the center frequency of the power spectrum at depth z [14].

In a manner similar to the methods that estimate the center frequency downshift, the SCC method measures the spectral shift of entire power spectra and estimates the slope of spectral shift instead of the slope of downshift of the center frequency. Because the attenuation is linearly proportional to the derivative of the center frequency with respect to the distance (depth), as shown in (7), the absolute estimation of the center frequency of the backscattered RF signals is not required for the estimation of the attenuation coefficient.

In order to estimate the attenuation coefficient, as shown in (7), the variance of a transmit pulse, σ^2, is necessary. In addition, diffraction effects for focused array transducers have to be considered for accurate estimation of the attenuation coefficient, since diffraction of the acoustic wave distorts the spectral characteristics with depth [19]. In the next subsection, we describe a method utilized for estimating the variance of the transmit pulse and the compensation for diffraction effects. Details of the ultrasound simulation program are also described in the next subsection.

TABLE I
Transducer Simulation Parameters.

Transducer type	Linear array
Element size	0.2 mm × 10 mm
Number of elements	128
Element spacing	0.2 mm
F-number	2
Center frequency	5 MHz
Bandwidth	50%
Beam focus	40 mm

A. Ultrasound Simulation Procedure

RF echo signals for both the reference and the sample phantom with various attenuation coefficients and transducer properties were generated using an ultrasound simulation program [25]. This program is a frequency-domain model based on classical diffraction theory for continuous wave propagation [26].

For this study, a linear array transducer consisting of elements of size 0.2 mm by 10 mm, with a center-to-center distance of 0.2 mm, was utilized. Each beam line was formed using 128 consecutive elements. The elevational focus was set to be the same as the lateral transmit focus. A dynamic receive focus and dynamic aperture were utilized such that the F-number was fixed at 2. The ultrasound field varied with axial distance from the transducer. A Gaussian-shaped pulse with a center frequency of 5 MHz and a bandwidth of 50% was used as the incident pulse. The transducer simulation parameters are summarized in Table I.

Two uniform phantoms were simulated by randomly distributing 50-μm polystyrene beads and 25-μm glass beads in a medium that had a sound speed of 1540 m/s. The scatterer number density was set at 9.686 per cubic millimeter, which simulates Rayleigh scattering. The modeled phantom dimensions were 40 mm (width) by 80 mm (height) by 10 mm (thickness), and the distance between adjacent beam lines was fixed at 0.2 mm. The center of the phantom was placed at a 40-mm depth from the transducer, which coincided with the transmit and receive foci.

After generating simulated RF data with a specified value of the attenuation coefficient, the entire RF data frame was divided into smaller overlapping two-dimensional (2-D) blocks of sufficient size to obtain a consistent power spectrum. The block power spectrum was calculated using the short-time Fourier analysis technique by averaging spectra from the windowed segments within the block [27]. In each 2-D block, the gated window size

was set to half the axial length of the block, with a 50% window overlap used to calculate the block power spectrum. Each windowed RF segment was gated by a Hanning window to minimize spectral leakage artifacts. Each block contained 10 beam lines in the lateral direction with each block power spectrum obtained from an average of 30 Fourier spectra. A 50% overlap of the 2-D block was applied in axial and lateral directions to obtain spectral shift estimates. Frequency smoothing, where adjacent frequency estimates are averaged using a moving window [28], was also utilized to further reduce spectral noise artifacts in the power spectra.

After estimating the block power spectra from the gated echo signals, the SCC algorithm [18] was utilized to compute the spectral shift between two consecutive power spectra. The spectral shift was obtained from the location of the maximum of the cross-correlation function. (In (5), this location is obtained using the derivative of $S(f_o)$ with respect to f_o). The spectral shift is equivalent to the center frequency downshift obtained from two consecutive centroid estimates.

Since the block power spectra are quite noisy in the frequency domain, we set a threshold using the cross-correlation coefficient value as a quality parameter. If the maximum cross-correlation coefficient was smaller than the threshold, the spectral shift obtained using the SCC method was ignored and replaced with an interpolated result from surrounding spectral shift estimates. Local attenuation coefficient estimates were computed using a linear regression of the shift estimates with a specified size of the linear fit window. The final estimated attenuation coefficient was calculated using (7).

B. Estimation of Transmit Pulse Properties

In general, the shape of transmit pulse is assumed to be Gaussian at the center frequency; however, exact information such as the bandwidth specified by the full-width half-maximum (FWHM) or the variance of the transmit pulse is not available in most ultrasound pulse-echo systems. In this paper, we estimated the variance of transmit pulse by calculating the FWHM from the power spectrum of the backscattered RF signals. Since the relationship between FWHM and the variance of Gaussian distribution is known, the estimated FWHM is converted into a variance measure to calculate an estimate of the attenuation coefficient.

The FWHM of the block power spectrum in our simulation was calculated by the ratio of half-power bandwidth and center frequency from the power spectrum of the echo signal. Many ultrasound pulse-echo systems utilize this ratio to represent the pulse bandwidth. The measured FWHM of power spectra along depth, which had a 0.5-dB/cm/MHz attenuation coefficient and a 5-MHz center frequency with 0.5 FWHM, are shown in Fig. 1. Although the measured FWHM fluctuates at different depths, the average FWHM is similar to the original FWHM in the simulation results. Therefore, the average measured FWHM was used to model the characteristics of the transmit pulse to calculate the attenuation coefficient in (7).

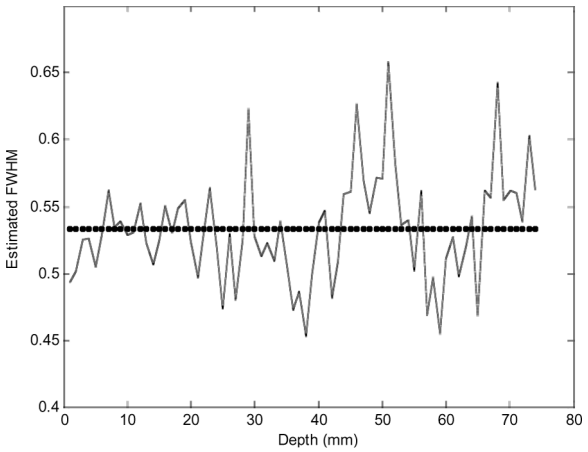

Fig. 1. Estimated FWHM of the power spectrum from the backscattered echo signal. The center frequency of the transmit pulse is 5 MHz and FWHM is 0.5. The attenuation coefficient of the phantom is 0.5 dB/cm/MHz. The mean of the measured FWHM is plotted as the dotted line.

C. Diffraction Compensation

Since most linear array transducers in ultrasound pulse-echo systems utilize focusing to obtain better B-mode images around the region of interest, echo signals acquired by focused transducers contain diffraction effects around the pre- and post-focal sections of the B-mode image. Due to acoustic diffraction effects, spectral properties of the power spectra are distorted and the attenuation estimate obtained is also affected as the ultrasound signal propagates along the axial direction. Fink *et al.* [19] studied diffraction effects using classical sound theory and focused transducer models, and reported that the estimated attenuation coefficients were underestimated at pre-focal regions and overestimated in the post-focal regions.

To compensate for diffraction effects in estimating the attenuation coefficient, we propose a simple method based on the use of a uniform reference phantom with a known attenuation coefficient. Backscattered RF signals are acquired from both the reference and the sample phantoms with the same transducer settings (i.e., same focus, same TGC, same beam pattern, etc.). Since the attenuation coefficient of the reference phantom is known, the theoretical downshift of the center frequency along depth can be easily calculated. This theoretical center frequency downshift would be a straight line whose slope is proportional to the attenuation coefficient. However, the measured experimental center frequency changes of an actual reference phantom would be distorted due to beam focal properties.

By comparing center frequency changes along the depth between the theoretical and measured values in the reference phantom, the contributions due to diffraction effects on the center frequency can be estimated. The center frequency difference between the theoretical and measured

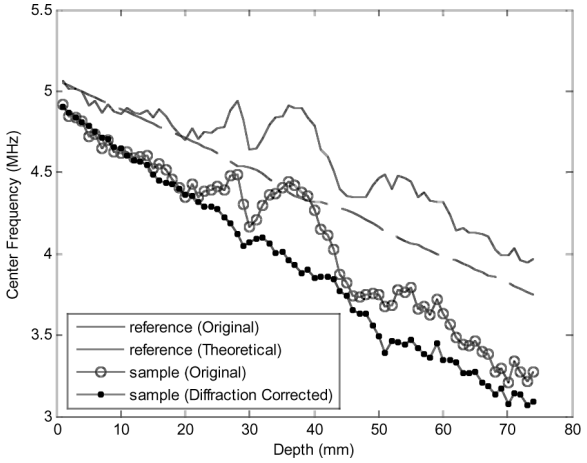

(a)

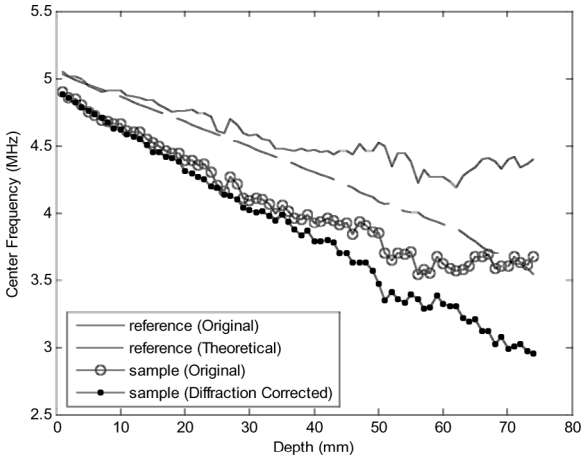

(b)

Fig. 2. Diffraction compensation with respect to the reference echo signal. The attenuation coefficients of the reference and the sample are 0.3 dB/cm/MHz and 0.5 dB/cm/MHz, respectively. (a) Beam focus is at 40 mm. (b) Beam focus is at 80 mm.

values are normalized with respect to frequency at each depth in the reference phantom and utilized for diffraction correction in the sample phantom. Since the same transducer settings are utilized for both reference and sample, diffraction effects also demonstrate similar behavior for the reference and sample.

Fig. 2 shows the changes in the center frequency estimates before and after diffraction compensation of the reference and sample echo signals. The attenuation coefficient of the reference was 0.3 dB/cm/MHz and that of the sample was 0.5 dB/cm/MHz, and total axial depth of phantom was 8 cm. The transducer focus was at 40 mm and 80 mm, respectively. The transmit pulse was assumed to follow a Gaussian shape, and its center frequency was 5 MHz with a FWHM of 0.5. The theoretical slope of the reference echo signal is plotted as the dotted line. The measured (before diffraction compensation) center frequency changes for the reference and sample echo signals peak at the focus around 40 mm and 80 mm. However, after diffraction compensation, the center frequency changes observed in the sample are relatively linear along the depth scanned.

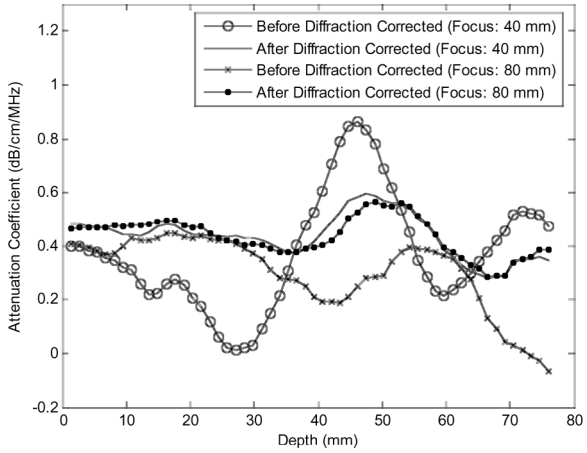

Fig. 3. Attenuation estimation with and without diffraction compensation. The attenuation coefficient of the sample is 0.5 dB/cm/MHz and a 0.3 dB/cm/MHz reference is used as the diffraction compensation for the SCC method. The size of the linear fit window is 15.6 mm.

The estimated attenuation coefficients with and without diffraction compensation are shown in Fig. 3. As expected from the center frequency curves in Fig. 2, the estimated attenuation coefficient without diffraction compensation before the focal region is underestimated and that beyond the focal region is overestimated. The results presented in this paper are similar to the simulation results for a focused transducer shown by Fink *et al.* [19]. However, since the slope of the diffraction-compensated center frequency of the sample is relatively constant, the estimated attenuation coefficient after diffraction compensation is independent of focusing effects and provides stable results along the entire depth scanned.

D. Gated Window Sizes for Power Spectrum Computation

For the computation of the power spectrum for a 2-D block, each A-line within the block was divided into smaller segments weighted by a Hanning window to minimize edge artifacts. Although a smaller size of the gated windows is preferred to provide better spatial resolution of the final attenuation estimate, it has to contain sufficient frequency information of the backscattered RF signal to provide robust power spectra. The ideal size of the gated window would be small enough to satisfy the stationarity assumption and provide sufficient spatial resolution of the attenuation estimate, but also large enough to generate an accurate and robust power spectrum of the backscattered RF signals. The number of wavelengths of the acoustic pulse within the gated window is another parameter that determines the necessary size of the gated window. Larger gated window sizes may also introduce additional errors due to the non-stationarity of the backscattered echo signals.

The attenuation estimation performance of different gated window sizes and number of windowed-segments within the block used to estimate the power spectrum from backscattered RF signals for the SCC method are evalu-

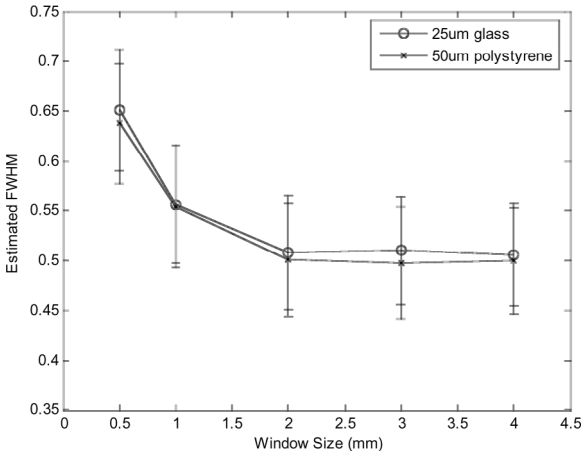

(a)

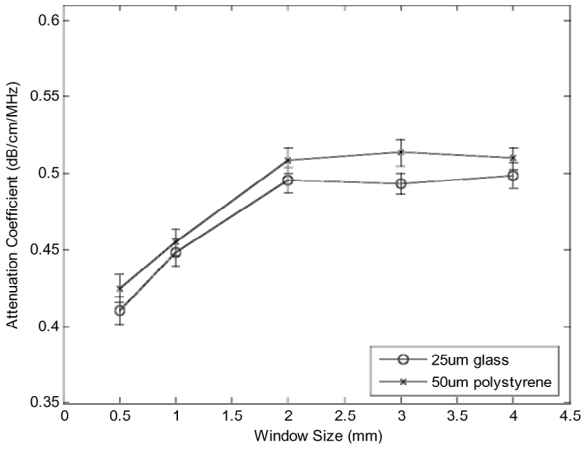

(b)

Fig. 4. Estimations of the FWHM and the attenuation coefficient with different gated window sizes. The lines with the open circles denote the phantom with the 25-μm glass beads and the lines with the crosses denote the 50-μm polystyrene beads. The number of averaged gated window power spectra in each block is 60. The error bars represent the standard deviations of estimated values. (a) The FWHM estimate from backscattered RF signals. The center frequency of the transmit pulse is 5 MHz and the actual FWHM is 0.5. (b) Attenuation estimates with different gated window sizes. The actual attenuation coefficient is 0.5 dB/cm/MHz. The window overlap between two adjacent window segments is 50% and the size of the linear fit window is 15.6 mm.

ated in this paper. Although it is difficult to ascertain the accuracy of the power spectrum, we used the estimated FWHM of the backscattered RF signal as a metric to evaluate the power spectrum. Accurate estimation of FWHM (or the variance of the transmit pulse) is one of the more important factors in the estimation of the attenuation coefficient as shown in (7).

If the size of the gated window is too small with respect to the center frequency of a transmit pulse, the estimated block power spectrum may be broadened and have a larger FWHM value. For a small gated window, therefore, the estimated power spectrum may not effectively represent the power distribution for the different frequency range, leading to an underestimation of the attenuation coefficient. Fig. 4 contains plots of the estimated FWHM of the backscattered RF signals and the resulting estimated attenuation coefficients for the 25-μm glass bead and 50-μm polystyrene bead sample phantoms. To obtain an estimate of the optimum gated window size, we estimated the attenuation coefficient over a range of window sizes, as shown in Fig. 4. The overlap ratio of adjacent gated windows was set to 50% and the number of averaged Fourier spectra to obtain the expected value or the power spectrum was set to a large value of 60 averages to obtain a consistent block power spectrum. All of the other signal processing parameters were maintained the same. As shown in Fig. 4(a), the estimated FWHM are larger for the smaller gated window sizes, and converge to the true value of the FWHM with an increase in the size of the gated window.

The estimated attenuation coefficients, shown in Fig. 4(b), also underestimate the actual value of the attenuation for small gated windows and stabilize for window sizes larger than 2 mm. Since the estimated attenuation coefficient is normalized by the variance of the transmit pulse, reliable estimation of the FWHM of the transmit pulse is important. Our simulation results in Fig. 4 demonstrate that the window size has to be greater than 2.0 mm or 7 wavelengths to obtain an accurate, stable, and robust power spectrum.

The number of independent gated window segments is another factor that is important in the estimation of the block power spectrum. The number of gated window segments used to obtain the block power spectra, in general, depends on both the window overlap and the lateral width of a block. In our results, the window overlap ratio was fixed at 50% and the lateral width of the block was increased to obtain a larger number of independent data segments. Fig. 5 illustrates the estimated attenuation coefficient versus the number of data segments for the 2.0-mm gated window size used to obtain the block power spectra. Note that as the number of segments was increased, the estimated attenuation values converged to the actual attenuation value. Our simulation results in Fig. 5 indicate that the number of segments within the data block has to be greater than 30 to obtain stable block power spectra.

IV. Simulation Results

As described in Section III, we simulated RF echo signal frames for two cases, one where the scatterers were represented by 25-μm glass beads and the second simulation utilizing 50-μm polystyrene beads. RF echo signal frames with three different values of the attenuation coefficient, namely, 0.3, 0.5, and 0.7 dB/cm/MHz, were obtained. These phantoms were utilized one as the reference and the other as the sample, respectively. The attenuation coefficients were calculated at two regions, chosen at different depths in the phantom. Region A was selected to be close to the transducer face (around 1 cm–3 cm), while region B was in the far-field (around 5 cm–7 cm). The 2-D block sizes for the power spectra were selected to be 2×2 mm, 3×2 mm, and 4×2 mm along the axial

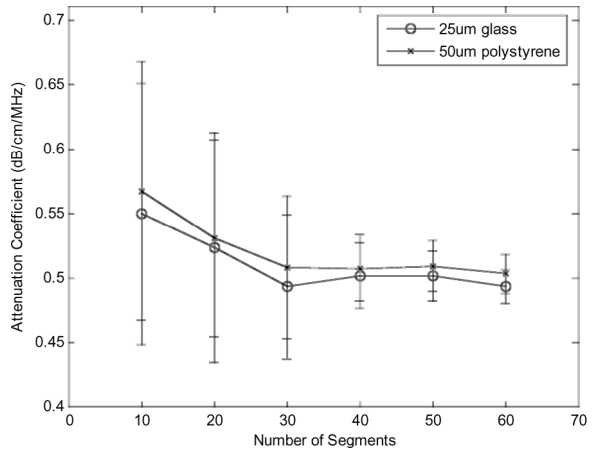

Fig. 5. Attenuation estimates obtained with different numbers of gated data segments within the block power spectrum. The line with the open circles denotes the 25-μm glass beads and the line with the crosses denotes the 50-μm polystyrene beads. The gated window size is 2.0 mm. The window overlap between two adjacent window segments is 50% and the size of the linear fit window is 15.6 mm. The error bars represent the standard deviations of estimated values.

TABLE II
ESTIMATED ATTENUATION COEFFICIENT (DB/CM/MHZ).

Reference : 0.3 vs. Sample : 0.5				
Block size		$2 \times 2 \times 1$	$3 \times 2 \times 1.5$	$4 \times 2 \times 2$
25-μm glass	region A	0.4766	0.4872	0.4914
	region B	0.4139	0.4527	0.4669
50-μm polystyrene	region A	0.4646	0.4823	0.4907
	region B	0.3920	0.4292	0.4569
Reference : 0.5 vs. Sample : 0.7				
Block size		$2 \times 2 \times 1$	$3 \times 2 \times 1.5$	$4 \times 2 \times 2$
25-μm glass	region A	0.6783	0.6879	0.6921
	region B	0.6157	0.6539	0.6671
50-μm polystyrene	region A	0.6655	0.6829	0.6911
	region B	0.6141	0.6445	0.6598

and lateral dimensions, respectively. The 2-D blocks were overlapped by 50% in both directions to estimate consecutive power spectra and compute the attenuation coefficient. Gated window sizes in each block were chosen to be half the axial length and overlapped by 50% in the axial direction. Each block power spectrum, therefore, was obtained from 30 Fourier spectra. Frequency smoothing was also applied to the time-averaged power spectrum to reduce spectral noise artifacts.

The estimated attenuation coefficients using the SCC method are shown in Table II. In the row denoting the block size, "$2 \times 2 \times 1$" represents a 2-mm (axial) by 2-mm (lateral) block with a 1-mm gated window. Note that although the attenuation coefficients are underestimated in region B in Table II, the estimated attenuation coefficient values are fairly close to the actual value. Observe that while the estimated attenuation coefficients are underestimated for the smaller block and window sizes, as expected, they converge to the actual value with an increase in the block and window sizes. With an appropriate choice of the gated window size, the mean attenuation coefficient obtained is within 2.35% and 2.25% of the actual values, respectively.

TABLE III
ESTIMATION VARIANCE.

Reference : 0.3 vs. Sample : 0.5				
Block size		$2 \times 2 \times 1$	$3 \times 2 \times 1.5$	$4 \times 2 \times 2$
25-μm glass	region A	0.0332	0.0245	0.0199
	region B	0.0522	0.0311	0.0331
50-μm polystyrene	region A	0.0347	0.0331	0.0344
	region B	0.0425	0.0293	0.0261
Reference : 0.5 vs. Sample : 0.7				
Block size		$2 \times 2 \times 1$	$3 \times 2 \times 1.5$	$4 \times 2 \times 2$
25-μm glass	region A	0.0325	0.0228	0.0192
	region B	0.0536	0.0324	0.0330
50-μm polystyrene	region A	0.0352	0.0335	0.0363
	region B	0.0395	0.0243	0.0241

Backscattered ultrasound RF signals contain speckle noise artifacts due to the generation of the echo signal from an ensemble of scatterers. For smaller gated window sizes, these noise artifacts introduce additional errors. Therefore, in addition to the accuracy of the estimated attenuation coefficient, the precision (or estimation variance) is another important metric used to characterize the estimation method.

Table III shows the estimation variance of the SCC method for 31 small blocks of the uniform attenuation region. The estimation variances are relatively small and independent of the region used in the measurement. Although the gated window size varied, the estimation variances did not change significantly in our simulation results. Attenuation coefficients estimated using simulations along the entire beam path are shown in Fig. 6. We estimated the attenuation coefficient using spectral cross-correlation algorithm with a small estimation variance that is not dependent on the propagation depth and beam focal properties.

V. EXPERIMENTAL RESULTS

In addition to the simulated RF echo signals, two tissue-mimicking (TM) phantoms manufactured in our laboratory were also used to test the proposed SCC algorithm. One of the phantoms was a uniform reference phantom, consisting of 45 to 53-μm glass beads in a gelatin background, with an attenuation coefficient of 0.5 dB/cm/MHz [29]. The other was a sample phantom, referred to as the attenuation phantom (AP), which contained two cylindrical inclusions with 20-μm glass beads in the background and a 0.5 dB/cm/MHz attenuation coefficient. Both of the inclusions had higher attenuation coefficients

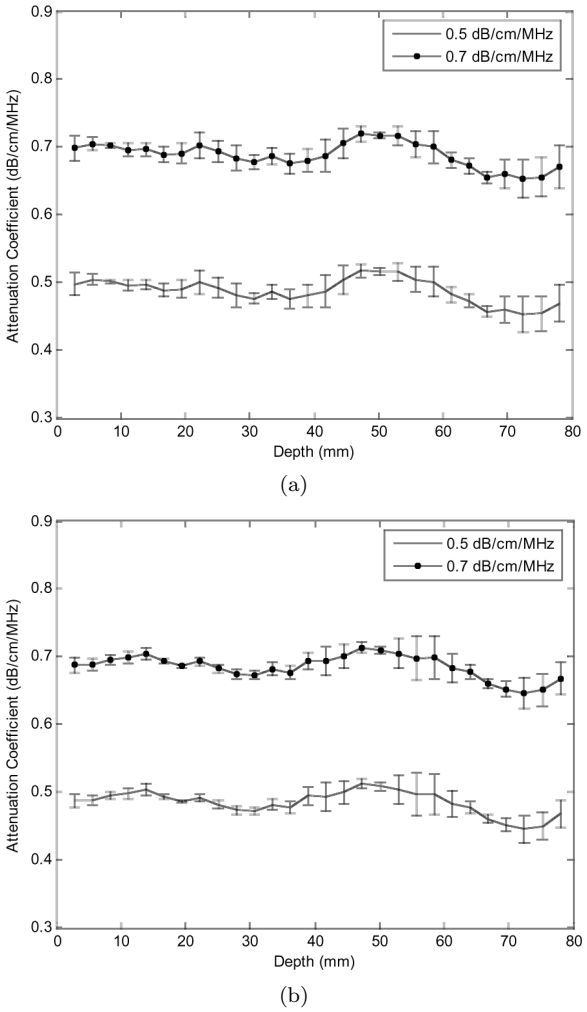

Fig. 6. Attenuation coefficient estimates for simulated uniform phantoms along the entire beam path using the spectral cross-correlation algorithm. A block size of 4 mm (axial) by 2 mm (lateral) with a 2-mm window size is used to compute the power spectrum. The size of the linear fit window is 15.6 mm. The attenuation coefficients of the reference are 0.3 and 0.5 dB/cm/MHz and those of the sample are 0.5 and 0.7 dB/cm/MHz. The error bars denote the estimation variances for the (a) 25-μm glass bead and (b) 50-μm polystyrene bead scatterers.

of 0.8 dB/cm/MHz, when compared to the background. The backscatter coefficient of the right inclusion was the same as that of the background material, while that of the left inclusion was 3 dB higher than that of the background.

The TM phantoms were scanned using a Siemens Antares ultrasound system (Siemens Medical Systems, Issaquah, WA) using a linear array transducer at a 4-MHz center frequency. The AP was scanned at three different regions: namely, the uniform background region without the inclusion, and the left and right inclusion regions. RF data from each of these regions were acquired at five independent locations along the cylindrical inclusion, and block power spectra of each region were averaged to improve the statistical accuracy.

Table IV shows the attenuation estimates obtained with the TM phantoms. Two different block and gated window sizes were tested, and the estimated attenuation coefficients of all blocks were averaged within a 2 cm $\times$ 1 cm region of each target. The left column shows the scanned regions, and estimation variances are shown in parenthesis. For the uniform background region, AP_UNI, the estimated attenuation coefficients are closer to the actual value for both block sizes utilized. However, the smaller block underestimates the attenuation coefficient in the inclusion regions, similar to the simulated RF data cases. For the inclusion with the higher backscatter coefficient, AP_LEFT, the attenuation coefficients were overestimated because of the frequency dependence of the backscatter. Techniques to minimize the impact of variation in the backscatter coefficient have to be considered.

TABLE IV
ESTIMATED ATTENUATION COEFFICIENTS OF TISSUE MIMICKING PHANTOM (DB/CM/MHZ).

Block size	$2 \times 2 \times 1$	$4 \times 2 \times 2$
AP_UNI	0.4989 (0.0017)	0.4970 (0.0081)
AP_LEFT	0.7150 (0.0009)	1.0537 (0.0088)
AP_RIGHT	0.6293 (0.0017)	0.8284 (0.0187)

VI. CONCLUSION

Estimation of the ultrasound attenuation coefficient in soft tissues is crucial not only for clearer understanding of the clinical features but also for further analysis of B-mode images. Since the backscattered ultrasound RF signals include noise artifacts due to inhomogeneous tissue structure and transducer-dependent parameters, it is difficult to extract spectral properties from the backscattered RF signals. In addition, diffraction effects with focused transducers also distort the spectral characteristics of the received echo signals.

In this paper, we propose the use of the SCC method in the frequency domain for estimating the spectral shift between consecutive power spectra. Since the SCC method calculates the spectral downshift of the entire power spectra, it provides accurate and stable estimation of the shift in frequency domain. In addition, we propose a simple diffraction correction technique using data obtained from a reference phantom. The diffraction correction method compensates for transducer dependent parameters, especially beam focusing effects on the attenuation coefficient estimate. Selection of appropriate gated window sizes, and number of independent Fourier spectra to obtain the power spectra are other factors that impact the performance of the SCC method in estimating the attenuation coefficient. In this paper, we provide guidelines for the selection of gated window sizes using the FWHM of backscattered RF signals.

Simulation results demonstrate the accuracy of the SCC method for the estimation of the attenuation coefficients. The mean attenuation coefficient obtained using the SCC method was within 2.3% of the actual value with a small

estimation variance for simulated RF data. The estimated attenuation coefficients for TM phantoms are also closer to the actual values with small estimation variance.

Appendix A
Attenuation Estimation Using Spectral Cross-Correlation

The cross-correlation function between the two power spectra at different depths, z_1 and z_2 ($z_1 < z_2$), from (5) can be written as

$$S(f_o) = \int_{-\infty}^{\infty} R(f + f_o, z_1) \cdot R(f, z_2) df, \tag{A1}$$

where f_o denotes the spectral shift. Assuming that the attenuation coefficient does not change abruptly within the small region of interest, and z_1 and z_2 are close to each other, the attenuation coefficients at depth z_1 and z_2 can be assumed to be similar. Substituting (1), for $R(f, z)$, into the above equation and simplifying, we obtain

$$S(f_o) = \int_{-\infty}^{\infty} \big[G(f + f_o) \cdot A(f + f_o, z) \cdot B(f + f_o) \cdot G(f) \cdot A(f, z) \cdot B(f)\big] df. \tag{A2}$$

Substituting for $G(f)$, $A(f, z)$, and $B(f)$ from (2), (3), and (4) in (A2), we obtain

$$S(f_o) = \int_{-\infty}^{\infty} \left[\exp\left\{-\frac{(f + f_o - f_c)^2}{2\sigma^2}\right\} \cdot \exp\{-4\beta(f + f_o)z_1\} \cdot (f + f_o)^n \cdot \exp\left\{-\frac{(f - f_c)^2}{2\sigma^2}\right\} \cdot \exp\{-4\beta f z_2\} \cdot f^n \right] df. \tag{A3}$$

After replacing $f^n \cdot (f + f_o)^n$ with the exponential form of the Taylor series expansion,

$$S(f_o) = \int_{-\infty}^{\infty} \left[\exp\left\{-\frac{(f + f_o - f_c)^2}{2\sigma^2}\right\} \cdot \exp\{-4\beta(f + f_o)z_1\} \cdot \exp\left\{-\frac{(f - f_c)^2}{2\sigma^2}\right\} \cdot \exp\{-4\beta f z_2\} \cdot \exp\left\{-\frac{n \cdot \{2f^2 + (2f_o - 8f_c)f + f_0^2 - 4f_c f_o\}}{2f_c^2}\right\} \right] df. \tag{A4}$$

Simplifying, we obtain

$$S(f_o) = \int_{-\infty}^{\infty} \exp\left[-\frac{A}{2\sigma^2 f_c^2}\right] df, \tag{A5}$$

where

$$A = 2B\left(f + \frac{C}{2B}\right)^2 + \frac{2BD - C^2}{2B} \tag{A6}$$

and

$$B = f_c^2 + n\sigma^2, \tag{A7}$$

$$C = Bf_o - 2f_c^3 + 4\sigma^2\beta(z_1 + z_2)f_c^2 - 4n\sigma^2 f_c, \tag{A8}$$

$$D = Bf_o^2 + 2(4\sigma^2\beta z_1 f_c^2 - f_c^3 - 2n\sigma^2 f_c)f_o + 2f_c^4. \tag{A9}$$

The SCC function can be written as

$$S(f_o) = \int_{-\infty}^{\infty} \exp\left[-\frac{\left(f + \frac{C}{2B}\right)^2}{\frac{\sigma^2 f_c^2}{B}}\right] \cdot \exp\left[\frac{C^2 - 2BD}{4\sigma^2 f_c^2 B}\right] df. \tag{A10}$$

Separating the terms from within the integral, we obtain

$$S(f_o) = \exp\left[\frac{C^2 - 2BD}{4\sigma^2 f_c^2 B}\right] \cdot \int_{-\infty}^{\infty} \exp\left[-\frac{\left(f + \frac{C}{2B}\right)^2}{\frac{\sigma^2 f_c^2}{B}}\right] df. \tag{A11}$$

Eq. (A11) is of the form $\int_{-\infty}^{\infty} \exp(-\alpha x^2) dx = \sqrt{\pi/\alpha}$.

Substituting and simplifying, we obtain

$$S(f_o) = \exp\left\{\frac{E}{4\sigma^2 f_c^2}\right\} \cdot \sqrt{\frac{\sigma^2 f_c^2 \cdot \pi}{B}}, \tag{A12}$$

where

$$E = \frac{C^2 - 2BD}{B}. \tag{A13}$$

In order to find the spectral shift, which occurs at the maximum of the cross-correlation function, we equate the derivative of $S(f_o)$ with respect to f_o to zero, i.e.,

$$\frac{dS(f_o)}{df_o} = \sqrt{\frac{\sigma^2 f_c^2 \cdot \pi}{B}} \cdot \exp\left\{\frac{E}{4\sigma^2 f_c^2}\right\} \cdot \frac{dE}{df_o} = 0. \tag{A14}$$

Simplifying, we obtain

$$-2B^2 f_o - 8B\sigma^2\beta(z_1 - z_2)f_c^2 = 0 \tag{A15}$$

or

$$f_{o(\max)} = \frac{4\sigma^2\beta(z_1 - z_2)}{1 + \frac{n\sigma^2}{f_c^2}}. \tag{A16}$$

Since the center frequency is generally greater than the square root of the variance of transmit pulse, and parameter n for human tissue is between 1 and 2, the spectral shift between the power spectra obtained at two different depths is linearly proportional to the attenuation coefficient and difference of the depths at which the spectra were obtained.

Acknowledgments

The authors acknowledge the efforts of the reviewers for their helpful comments and constructive suggestions for this paper. Their efforts have helped significantly in improving this paper.

References

[1] K. A. Dines and A. C. Kak, "Ultrasonic attenuation tomography of soft tissues," *Ultrason. Imag.*, vol. 1, pp. 16–33, 1979.

[2] G. Berger, P. Laugier, M. Fink, and J. Perrin, "Optimal precision in ultrasound attenuation estimation and application to the detection of Duchenne muscular dystrophy carriers," *Ultrason. Imag.*, vol. 9, pp. 1–17, 1987.

[3] B. J. Oosterveld, J. M. Thijssen, P. C. Hartman, R. L. Romijn, and G. J. Rosenbusch, "Ultrasound attenuation and texture analysis of diffuse liver disease: Methods and preliminary results," *Phys. Med. Biol.*, vol. 36, no. 8, pp. 1039–1064, 1991.

[4] G. Berger, P. Laugier, J. C. Thalabard, and J. Perrin, "Global breast attenuation: Control group and benign breast diseases," *Ultrason. Imag.*, vol. 12, no. 1, pp. 47–57, 1990.

[5] R. Kuc, "Bounds on estimating the acoustic attenuation of small tissue regions from reflected ultrasound," *Proc. IEEE*, vol. 73, no. 7, pp. 1159–1168, 1985.

[6] S. W. Flax, N. J. Pelc, G. H. Glover, F. D. Gutmann, and M. McLachlan, "Spectral characterization and attenuation measurements in ultrasound," *Ultrason. Imag.*, vol. 5, no. 2, pp. 95–116, 1983.

[7] H. S. Jang, T. K. Song, and S. B. Park, "Ultrasound attenuation estimation in soft tissue using the entropy difference of pulsed echoes between two adjacent envelope segments," *Ultrason. Imag.*, vol. 10, no. 4, pp. 248–264, 1988.

[8] B. S. Knipp, J. A. Zagzebski, T. A. Wilson, F. Dong, and E. L. Madsen, "Attenuation and backscatter estimation using video signal analysis applied to B-mode images," *Ultrason. Imag.*, vol. 19, no. 3, pp. 221–233, 1997.

[9] S. L. Baldwin, K. R. Marutyan, M. Yang, K. D. Wallace, M. R. Holland, and J. G. Miller, "Estimating myocardial attenuation from M-mode ultrasonic backscatter," *Ultrasound Med. Biol.*, vol. 31, no. 4, pp. 477–484, 2005.

[10] B. Zhao, O. A. Basir, and G. S. Mittal, "Estimation of ultrasound attenuation and dispersion using short time fourier transform," *Ultrasonics*, vol. 43, pp. 375–381, 2004.

[11] R. Kuc and H. Li, "Reduced-order autoregressive modeling for center-frequency estimation," *Ultrason. Imag.*, vol. 7, no. 3, pp. 244–251, 1985.

[12] L. X. Yao, J. A. Zagzebski, and E. L. Madsen, "Backscatter coefficient measurements using a reference phantom to extract depth-dependent instrumentation factors," *Ultrason. Imag.*, vol. 12, no. 1, pp. 58–70, 1990.

[13] L. S. Wilson, D. E. Robinson, and B. D. Doust, "Frequency domain processing for ultrasonic attenuation measurement in liver," *Ultrason. Imag.*, vol. 6, pp. 278–292, 1984.

[14] M. Fink, F. Hottier, and J. F. Cardoso, "Ultrasonic signal processing for in vivo attenuation measurement: Short time Fourier analysis," *Ultrason. Imag.*, vol. 5, no. 2, pp. 117–135, 1983.

[15] C. Kasai, K. Namekawa, A. Koyano, and R. Omoto, "Real-time two-dimensional blood flow imaging using an autocorrelation technique," *IEEE Trans. Sonics Ultrason.*, vol. 32, no. 3, pp. 458–464, 1985.

[16] T. Baldeweck, P. Laugier, A. Herment, and G. Berger, "Application of autoregressive spectral analysis for ultrasound attenuation estimation: Interest in highly attenuating medium," *IEEE Trans. Ultrason., Ferroelect., Freq. Contr.*, vol. 42, no. 1, pp. 99–109, 1995.

[17] J. Ophir, R. E. McWhirt, N. F. Maklad, and P. M. Jaeger, "A narrowband pulse-echo technique for in vivo ultrasonic attenuation estimation," *IEEE Trans. Biomed. Eng.*, vol. 32, no. 3, pp. 205–212, 1985.

[18] T. Varghese, E. E. Konofagou, J. Ophir, S. K. Alam, and M. Bilgen, "Direct strain estimation in elastography using spectral cross-correlation," *Ultrasound Med. Biol.*, vol. 26, no. 9, pp. 1525–1537, 2000.

[19] M. A. Fink and J. F. Cardoso, "Diffraction effects in pulse-echo measurement," *IEEE Trans. Sonics Ultrason.*, vol. 31, no. 4, pp. 313–329, 1984.

[20] K. A. Wear, "A Gaussian framework for modeling effects of frequency-dependent attenuation, frequency-dependent scattering, and gating," *IEEE Trans. Ultrason., Ferroelect., Freq. Contr.*, vol. 49, no. 11, pp. 1572–1582, 2002.

[21] P. He, "Acoustic attenuation estimation for soft tissue from ultrasound echo envelope peaks," *IEEE Trans. Ultrason., Ferroelect., Freq. Contr.*, vol. 36, no. 2, pp. 197–203, 1989.

[22] P. M. Shankar, "A general statistical model for ultrasonic backscattering from tissues," *IEEE Trans. Ultrason., Ferroelect., Freq. Contr.*, vol. 47, no. 3, pp. 727–735, 2000.

[23] G. Treece, R. Prager, and A. Gee, "Ultrasound attenuation measurement in the presence of scatter variation for reduction of shadowing and enhancement," *IEEE Trans. Ultrason., Ferroelect., Freq. Contr.*, vol. 52, no. 12, pp. 2346–2360, 2005.

[24] J. M. Girault, F. Ossant, A. Ouahabi, D. Kouame, and F. Patat, "Time-varying autoregressive spectral estimation for ultrasound attenuation in tissue characterization," *IEEE Trans. Ultrason., Ferroelect., Freq. Contr.*, vol. 45, no. 3, pp. 650–659, 1998.

[25] Q. Chen, "Computer simulations in parametric ultrasonic imaging," Ph.D. dissertation, Department of Medical Physics, University of Wisconsin-Madison, 2004.

[26] Y. Li and J. A. Zagzebski, "A frequency domain model for generating B-mode images with array transducers," *IEEE Trans. Ultrason., Ferroelect., Freq. Contr.*, vol. 46, no. 3, pp. 690–699, 1999.

[27] P. Welch, "The use of fast Fourier transform for the estimation of power spectra: A method based on time averaging over short, modified periodograms," *IEEE Trans. Audio and Electroacoustics*, vol. 15, no. 2, pp. 70–73, 1967.

[28] T. Varghese and K. D. Donohue, "Estimating mean scatterer spacing with the frequency-smoothed spectral autocorrelation function," *IEEE Trans. Ultrason., Ferroelect., Freq. Contr.*, vol. 42, no. 3, pp. 451–463, 1995.

[29] T. Wilson, J. Zagzebski, and Y. Li, "A test phantom for estimating changes in the effective frequency of an ultrasonic scanner," *J. Ultrasound Med.*, vol. 21, no. 9, pp. 937–945, 2002.

Hyungsuk Kim received the B.S. degree in Electrical Engineering at the Korea Institute of Technology, Daejeon, Korea, in 1991 and the M.S. degree in Image Processing and Pattern Recognition in Electrical Engineering at Seoul National University, Seoul, Korea, in 1993. From 1993 to 1999, he worked for Korea Telecom Research Group, Seoul, Korea, working on the design and analysis of data communication networks. Since 1999 he has been pursuing his Ph.D degree in Electrical and Computer Science at the University of Wisconsin-Madison, Madison, WI.

His current research interests are in signal processing applications in ultrasound including attenuation estimation in soft tissues, tissue characterization, and ultrasound image processing. Mr. Hyungsuk is a student member of the IEEE and the American Institute of Ultrasound in Medicine.

Tomy Varghese (S'92–M'95–SM'00) is currently an Associate Professor in the Department of Medical Physics at the University of Wisconsin-Madison. He received his Ph.D. in Electrical Engineering from the University of Kentucky, Lexington, KY, in 1995. His current research interests include elastography, ultrasound imaging, ultrasonic tissue characterization, detection and estimation theory, statistical pattern recognition, and signal and image processing applications in medical imaging.

He has worked on developing methods for the visualization of the treated region following radiofrequency ablation using elastographic and temperature imaging methods based on ultrasound. His work in developing ultrasound elastographic imaging techniques and ultrasonic tissue characterization has resulted in over 80 peer-reviewed journal publications, 8 patents, and several presentations in international conferences. Dr. Varghese is a senior member of the IEEE, the American Institute of Ultrasound in Medicine (AIUM), the American Association of Physicists in Medicine (AAPM) and Eta Kappa Nu.